A STATISTICAL STUDY OF SOLAR TYPE-III BURSTS AND AURORAL KILOMETRIC RADIATION ONSETS

by

William Michael Farrell

A thesis submitted in partial fulfillment
of the requirements for the Master of
Science degree in Physics
in the Graduate College of
The University of Iowa

December 1984

Thesis supervisor: Professor Donald A. Gurnett

Graduate College
The University of Iowa
Iowa City, Iowa

CERTIFICATE OF APPROVAL

MASTER'S THESIS

This is to certify that the Master's thesis of

William Michael Farrell

has been approved by the Examining Committee for the thesis requirement for the Master of Science degree in Physics at the December 1984 graduation.

Thesis committee: David A. Gruzalski
Thesis supervisor

Wayne Polzin
Member

Dwight Nicholaes
Member

ACKNOWLEDGEMENTS

The research at the University of Iowa was supported by contract NAS5-26819 with Goddard Space Flight Center, and by grants NGL-16-001-002 and NGL-16-001-043 from NASA Headquarters and by the Office of Naval Research.

I would like to thank Don Gurnett for project direction, guidance and encouragement. Also, I am grateful to Bob Stone and Bob MacDowall for their ISEE-3 3-D radio mapping experiment data and to Fred Scarf for his ISEE-3 plasma wave investigation data. Terry Averkamp and Larry Granroth also deserve thanks for valuable input on data reduction and analysis. John Birkbeck also deserves credit for a fine drafting job. I am particularly grateful to Kathy Kurth for the careful work and patience used in typing this thesis.

ABSTRACT

The simultaneous occurrences of Type-III solar radio bursts and auroral kilometric radiation were observed by Calvert using ISEE-1 spectrograms. He suggested that the incoming Type-III burst stimulates kilometric radiation onsets.

This paper presents a statistical study of the correlation between Type-III bursts and auroral kilometric radiation. A superposed epoch analysis is performed on 200 Type-III events. The Type-III bursts were detected by the ISEE-3 spacecraft on the sunward side of the earth while the IMP-8 spacecraft was used to detect onsets of kilometric radiation on the nightside of the earth. For each event, the intensities measured by ISEE-3 (Type-III intensities) were subtracted from the intensities measured by IMP-8 (Type-III and possible AKR intensities). The resulting intensities for each event were then added to all the other events to determine if kilometric radiation is consistently observed after a Type-III burst's passage. This analysis was performed at the frequencies of 100 kHz, 178 kHz and 500 kHz.

The results of this analysis show that a statistically significant correlation exists between incoming Type-III bursts from the sun and kilometric radiation from the earth. According to the results, almost 10% of incoming Type-III bursts stimulate kilometric radiation.

TABLE OF CONTENTS

LIST OF TABLES

LIST OF FIGURES

I. INTRODUCTION

In a previous paper, Calvert [1981a] suggests that incoming Type-III solar radio bursts stimulate auroral kilometric radiation (AKR). This paper will present a statistical study of the Type-III/AKR relationship using 200 Type-III events in a superposed epoch analysis. A comparison of pre-event and post-event intensities will be made to determine if AKR is consistently triggered during Type-III burst passages.

The earth is a strong source of radiation in the kilometric wavelength regime. This radiation is called auroral kilometric radiation. Auroral kilometric radiation is most intense at frequencies between 50-500 kHz [Dunkel et al., 1970; Gurnett, 1974]. The IMP-8 satellite, measuring the modulation of AKR intensities from spacecraft rotation, found a near-earth origin (~ 3 R_e) of AKR [Gurnett, 1974]. Gallagher and Gurnett [1979] using Hawkeye 1 and IMP-6 found the AKR source region to be between 2 and 3 R_e. In their study, a time-averaged power flux is calculated for locations around the earth. The total power is, then, found by integrating the average power flux over an earth-encompassing shell. For shells enclosing the AKR source regions, the total power is constant but for small shells not enclosing the source regions, the total power decreases

substantially. The AKR source region is found by noting the shell radius at which a decrease in power can be detected.

Gurnett [1974] found that most AKR occurrences are on the nightside of the earth (between 6 hour to 18 hour MLT) and that the radiation is emitted in a broad conical region centered on about 22 hours MLT. Figure 1 shows, quantitatively, the AKR ray paths and their refraction from the propagation cutoff surface (where the index of refraction goes to zero).

Auroral kilometric radiation tends to occur in intense bursts lasting a few hours. Figure 2 shows AKR emissions as seen by the IMP-6 satellite. The dark lines on the figure represent the average intensity while the dots give the largest intensities found in the averaging period. The bursty nature can easily be seen by the rapid fluctuations in intensity at each frequency. Also, Figure 2 shows that the intensity of radiation varies with the frequency. The detailed fine structure of AKR is illustrated by the frequency vs. time plot of Figure 3. Again, the intensity varies in both frequency and time with the emissions occurring in a narrow band that drifts in frequency. Calvert [1982] suggests a laser feedback model to explain AKR fine structure. According to the model, thin density enhancements are located in the AKR source region. Within these enhancements, low energy radio waves can be amplified, reflected (off the enhancement boundary), and reamplified. A wave will experience a high growth rate only if an integer number of half wavelengths fits across the enhancement width. This implies that amplification will

occur if all the reflected waves in a region of the enhancement constructively interfere. A quenching effect will occur in regions where reflected waves destructively interfere. This model then accounts for the fine structure of AKR, where the source of the intense frequency bands seen in Figure 3 are located at the constructive interference layers of the enhancement.

Hawkeye 1 [Gurnett and Green, 1978] and ISIS 1 [Benson and Calvert, 1979; Calvert, 1981b] data indicate that AKR is propagating in the free space R-X mode and is emitted nearly perpendicular from the magnetic field lines in the source region. The source region also has a diminished plasma density [Calvert, 1981c] with the electron plasma frequency, f_{pe}, well below the electron gyrofrequency, f_{ge}.

Gurnett [1974] found that the occurrence of AKR is associated with discrete auroral arcs. These arcs are generated by intense energetic (inverted-V) electrons that beam parallel to the auroral magnetic field lines. The relationship of AKR to inverted-V electron precipitation has been confirmed by Benson et al. [1980]. Most theories developed today make use of the free energy of the auroral electrons as the energy source. Melrose [1976] suggests that the inverted-V electron beam amplifies low level radiation via the Doppler-shifted beam cyclotron resonance $\omega \equiv n\omega_{ce} + k_{\parallel} v_b$. The newly amplified radiation is the AKR that is observed by satellites in the auroral region. Wu and Lee [1979] suggest that part of the incoming inverted-V beam gets reflected back out of the auroral region by pitch angle reflection, creating an enhanced loss cone distribution.

Using a relativistic cyclotron resonance, $\omega - k_{\parallel} v_{\parallel} = \omega_{ge}/\gamma$ where $\gamma = (1 - \frac{v^2}{c^2})^{-1/2}$, the loss cone distribution amplifies any low level radiation present in the source region. Omidi and Gurnett [1982] show positive growth rates in the AKR source region using the relativistic cyclotron resonance and measured S3-3 electron distribution functions. One should note that the relativistic cyclotron resonance condition used by Wu and Lee traces out an ellipse in velocity space which can lead to growth rates much larger than the nonrelativistic cyclotron resonance condition, $\omega - k_{\parallel} v_{\parallel} = \omega_{ge}$.

Gurnett [1974] found that the maximum AKR intensities were about 10^{-14} Wm^{-2} Hz^{-1} at 30 R_e. Assuming the effective bandwidth of the signal is 300 kHz and the radiation is emitted uniformly over a 6.5 SR solid angle (found from ray tracing), the maximum total power output is on the order of 10^9 watts. Gallagher and Gurnett [1979] show that the average power output of AKR is on the order of 10^7 watts. This makes the earth a very intense radio source, comparable to the intensity of Jupiter's decametric radiation.

Based on current understanding, the auroral region with inverted-V electrons present acts similar to an amplifier, increasing the signal of low intensity noise to very large levels. Assuming a cosmic background noise level of 10^{-20} to 10^{-18} Wm^{-2} Hz^{-1}, a gain of 80-100 dB is necessary in the amplification region [Calvert, 1982].

Solar flares often eject energetic particles into the solar wind. These streaming particles can be picked up by satellite particle detectors well past 1 A.U. The electrons ejected from the

flares have energies ranging from 1 keV to 100 keV which corresponds to electron velocities as high as 0.5 c.

The stream moving through the solar wind creates a bump-on-tail type electron distribution. As fast particles arrive before the slow particles in any given location, the electron configuration is unstable and plasma oscillations develop at the local plasma frequency, f_{pe}. With the arrival of slower electrons, the plasma oscillations are damped as the "bump" on the "tail" of the main distribution moves to lower velocities. Associated with the oscillations are electromagnetic waves (Type-III radiation) at f_{pe} and $2f_{pe}$. For frequencies less than 1 MHz, the $2f_{pe}$ emission appears to be the dominant component [Fainberg and Stone, 1974]. Figure 4 shows a qualitative radial profile of generated plasma oscillations at f_{pe} and electromagnetic radiation at f_{pe} and $2f_{pe}$.

Since the plasma frequency, f_{pe}, decreases as the distance from the sun increases, a receiver will pick up a Type-III radio signal that drifts from high to low frequency in time. This variation of the spectrum from high to low frequencies characterizes the Type-III burst [Wild, 1950]. Figure 5 shows a burst as detected by Helios-2. The radio burst is the smooth emission at 178 kHz and 100 kHz while the local electron plasma oscillation occurs at 56.2 kHz and 31.1 kHz. Figure 6 shows the Type-III burst as seen by ISEE-1 with the high to low frequency drift appearing on the spectrogram.

Solar Type-III bursts and AKR were believed to be unrelated phenomena until Calvert [1981a] noticed the simultaneous occurrences

of the two emissions using ISEE-1 spectrograms. Figure 7 shows an example of simultaneous Type-III events and AKR bursts. Note that the start of two of the AKR events corresponds to the passage of Type-III bursts. This simultaneity lead Calvert to believe the incoming Type-III bursts stimulate AKR onsets.

A model by Calvert suggests that the incoming Type-III radiation is refracted into the auroral zone by a decrease in plasma density. The radiation then passes through the AKR source region just about perpendicular to the magnetic field. The EM wave undergoes mode splitting that has an X-mode polarized component (the proper polarization needed for electron resonance) and an enhanced loss cone electron distribution, unstable to the wave, creates wave growth which can then be detected as intense AKR.

A question that must be asked is whether the simultaneous occurrence of the Type-III burst and AKR is accidental (is it random chance the two emissions are aligned as seen in Figure 7) or is there really a stimulation taking place (as Calvert's model suggests)? Calvert did a study in which independent, isolated Type-III bursts were checked for AKR onsets. ISEE-3, located at the libration point on the sunward side of the earth (0.1 A.U.), can detect Type-III bursts independent of AKR (for AKR occurs mainly on the nightside of earth). Corresponding ISEE-1 spectrograms were then checked for possible AKR onsets. Out of 27 Type-III bursts checked, 8 showed AKR onsets within 30 minutes after the Type-III burst's passage. In general, the average AKR onset rate per random 30-minute interval is

0.2 onsets per hour (or one AKR onset every 5 hours). The 30-minute interval after the Type-III's passage is more active with an AKR onset rate of 0.6 onsets per hour (i.e., 8/27 onsets in the 30-minute interval after the Type-III's passage). The increase in rate is attributed to Type-III stimulation of AKR [Calvert, 1981b]. This survey indicates that the simultaneity of Type-III bursts and AKR, as observed by Calvert, is not accidental, but is the result of a correlated occurrence of the two events.

The above survey has but one objection. A certain amount of subjectivity is present in the identification of the AKR onset from ISEE-1 spectrogram inspection. One must, first, identify the onset, then check if it is within 30 minutes of the Type-III's passage. Both identification and timing check are prone to human error.

This paper will present a survey in which 200 Type-III bursts have been checked for AKR onsets using an automated superposed epoch analysis procedure. In this study, ISEE-3 is used to identify Type-III bursts while IMP-8 is used to detect corresponding AKR onsets. The value of this survey is that the processing is done entirely by a computer with no subjective judgement on AKR onsets. This survey will make a comparison between the intensities of the isolated Type-III burst (detected by ISEE-3) to the Type-III burst and possible AKR onsets (detected by IMP-8) for each individual event. This comparison will be carried out at three frequencies: 100 kHz, 178 kHz, and 500 kHz.

II. SPACECRAFT INSTRUMENTATION

During this study, the ISEE-3 spacecraft was located at the libration point approximately 0.1 AU on the sunward side of the earth. From this position, ISEE-3 can easily detect incoming Type-III radio bursts independent of AKR (since AKR occurs mostly on the nightside of the earth). The ISEE-3 three-dimensional (3-D) radio mapping experiment and the ISEE-3 plasma wave investigation were used for Type-III detection in this survey.

The ISEE-3 3-D radio mapping experiment uses two electric dipole antennas, one in the spacecraft spin plane (90m tip-to-tip) and one along the spin axis (15m tip-to-tip) and are designated the S and Z antennas, respectively. The experiment is designed to study the coronal magnetic field and solar wind structure by tracking the 3-D trajectory of Type-III bursts. The modulation in intensity of the signal received by the S antenna can locate the azimuthal direction of arrival of a Type-III burst while signals from the S and Z antenna can locate the elevation. Each antenna drives two radiometers (one of 10-kHz bandwidth and one of 3-kHz bandwidth) and each radiometer steps through 12 frequencies (a different set of 12 for each radiometer) in a range from 30 kHz to 2 MHz [Knoll et al., 1978].

The 3-D radio mapping data is available on magnetic tape and consists of 108-second averaged power flux measurements from the S and Z antennas for the frequencies stepped through by the radiometers. Of particular interest are the S antenna intensities measured at the 513-kHz and the 188-kHz frequency channels, since these frequencies are nearly the same as used on IMP-8. The measurements at these frequencies will be used, in conjunction with the 500-kHz and 178-kHz IMP-8 channels, in this study.

The ISEE-3 plasma wave investigation uses 3 electric dipole antennas, two of 90m tip-to-tip length (the U and V antennas in the spin axis) and one of 0.6m effective length (on the X-axis of the spacecraft). Also, a search coil magnetometer is available to measure magnetic field strengths. The experiments in the plasma wave investigation are designed to gain information on plasma wave-particle interactions. A 16-channel spectrum analyzer with a frequency range of 17 Hz to 100 kHz is used to analyze the signals received from the long antennas. The analyzer can scan the frequency range every 0.5 seconds [Scarf et al., 1978].

The plasma wave data is also available on magnetic tapes and consists of intensity measurements taken every 1/2-second at each of the 16 channels measured by the spectrum analyzer. Measurements at 100 kHz are used in this survey because IMP-8 has a corresponding 100-kHz channel.

The IMP-8 spacecraft is in an earth orbit with a perigee radial distance of 147,343 km, an apogee radial distance of 295,054 km and

an orbital period of 11.98 days. This orbit takes IMP-8 through regions where AKR can be detected (i.e., nightside of earth). The electric dipole antennas (E_x and E_y) have a tip-to-tip length of 121.8m, but mechanical failure caused only the E_y to have its maximum length. The spectrum analyzer has fifteen channels for electric field measurements covering a frequency range of 40 Hz to 178 kHz with each channel being sampled every 10.24 seconds. In addition, a wideband receiver is available which can provide measurements over a frequency range from 10 Hz to 1 kHz. It can also be tuned to frequencies of 2.0 MHz, 500 kHz, 125 kHz, and 31.25 kHz where the receiver can act like another bandpass channel. For the period of time covering this survey, the wideband receiver was tuned to the 500-kHz channel.

The University of Iowa has made data tapes that average the intensities measured by the spectrum analyzer over 160-second intervals. These "IMP-8 compressed" tapes contain average and peak intensity measurements in 160-second intervals at each of the 16 frequency channels measured. The 100-kHz, 178-kHz and wideband (500-kHz) frequency channels are specifically used in this study.

III. ANALYSIS PROCEDURE

The first step in this study is to randomly select a set of Type-III bursts. From this set, a comparison of the intensity measurements from the two satellites will then determine if AKR is consistently triggered by Type-III bursts. Using the ISEE-3 survey books, 200 independent Type-III bursts were catalogued with the following criterion:

1) that the burst be isolated (i.e., no strong signals 1 hour before or after the burst);

2) and, that IMP-8 be on the nightside of the earth (between 6 hours and 18 hours MLT) when the burst passes. This is done to enhance the likelihood of detecting any stimulated AKR.

The beginning of each Type-III burst, at each of the three frequencies, was defined as $t = 0$ and the spectral density was examined 1 hour before and 1 hour after $t = 0$ for bursts detected by both ISEE-3 and IMP-8. For an event detected by ISEE-3, only background radiation intensities are measured the first hour ($t < 0$), while the second hour ($t > 0$) contains both background and Type-III burst intensities. The same event detected by IMP-8 measures background intensities the first hour while the second hour measurements contain background, Type-III, and any stimulated AKR intensities. The background level defined here does not refer to the usual cosmic

background emission but refers to any random occurring emission found for $t < 0$. Averaged over many events this "background" should be close to constant in time.

The 2-hour interval, measured by each spacecraft, is divided into equally spaced time bins. An average intensity for each time bin was found by summing the intensity measurements (with a computer) that have times that fall within the bin and dividing this sum by the number of measurements that fall into the bin (i.e., if the bin is 320 seconds long, two IMP-8 intensity measurements fall into the bin and the average intensity of the bin is the sum of these two measurements divided by two). This averaging process was carried out for measurements made by ISEE-3 and IMP-8. For each event, the average intensity measured in each time bin for the ISEE-3 measurements are then subtracted from the corresponding bin average intensities measured by IMP-8. In effect, the Type-III burst (measured by ISEE-3) is subtracted out of the combined Type-III/AKR emission (measured by IMP-8). Thus, after subtraction, the intensity of background radiation and any AKR onsets (found in $t > 0$) is left for each event.

Since spectral density measurements from ISEE-3 are subtracted from IMP-8, it is very important that the intensity calibration of the E-field detection instruments on both satellites be the same. To verify that instruments on both satellites give similar intensity measurements (for similar phenomenon), the spectral density of an isolated Type-III event (without AKR onsets) measured by IMP-8 was compared to the spectral density of the same event measured by ISEE-3.

If the intensity calibrations on both satellites are correct, the ratio of intensities of the Type-III bursts (with background subtracted off) measured by both spacecraft should be close to unity. The intensities measured by each satellite are compared by plotting the intensities on a log-log plot. Figures 8, 9, and 10 show the comparison of intensities for isolated Type-III events at each frequency. Figure 8 shows the comparison of intensities for the isolated Type-III event on Sept. 6, 1978, at 5:59 UT for 100 kHz. Figure 9 and Figure 10 show the comparison of intensities for the isolated Type-III event on June 26, 1979, at 14:55 UT for 178 kHz and 500 kHz. Note that the ratio of intensities is close to unity. The best fit linear relationship between the points is shown by the straight line. These plots (and others like them) confirm that ISEE-3 and IMP-8 measure essentially the same intensities. Most points on the figures are found to be within ±10% from linearity.

The above mentioned IMP-8 measurements (with Type-III burst intensities subtracted out) can now be added up, bin by bin, over all 200 events. This procedure is known as a superposed epoch analysis and yields a final distribution that is made up of the background and the possible AKR stimulated by Type-III bursts from all the events added together. If the AKR events are not correlated with Type-III bursts, there is an equal probability of AKR occurrences in the first hour ($t < 0$) as in the second ($t > 0$) and no major intensity increases should occur for $t > 0$. On the other hand, if the Type-III/AKR events are correlated, the latter hour ($t > 0$) should be of greater intensity than the first hour. This increase in intensity occurs because the first hour

measures background intensities only while the second hour measures background intensities plus the effect of the correlated occurrences of AKR.

The statistical analysis takes the following steps:

1) Averages are found for the first hour (background) and second hour (background and possible AKR onsets) from the final distribution. The averages for the first and second hour will be represented by $\overline{I}_{t<0}$ and $\overline{I}_{t>0}$, respectively.

2) The standard deviation of the mean (SDM) is calculated for the first hour. The SDM represents the deviation in a group of averages calculated from new sets of data. If one thinks of doing this survey over again many times with new sets of data, many new first hour averages will be calculated. The distribution of these averages has a standard deviation equal to the SDM. The SDM for the first and second hour will be represented by $SDM_{t<0}$ and $SDM_{t>0}$, respectively.

3) A variable ΔI will be defined where $\Delta I = \overline{I}_{t>0} - \overline{I}_{t<0}$. This represents the intensity increase from first to second hour.

4) Assuming no Type-III/AKR correlation exists, a variable ΔI_o is defined where $\Delta I_o = \overline{I}_{t>0} - \overline{I}_{t<0}$ with a hypothetical $\overline{I}_{t>0}$ which has the same statistical properties as $\overline{I}_{t<0}$. This ΔI_o represents the change in intensity expected when no Type-III/AKR correlation exists. The variable ΔI_o will, then, have an average value equal to zero and a standard deviation of its values corresponding to $SDM_o = \sqrt{(SDM_{t>0})^2 + (SDM_{t<0})^2}$ $= \sqrt{2}\ SDM_{t<0}$ ($SDM_{t<0} \cong SDM_{t>0}$ since background radiation is the only emission detected in the 2-hour period). A Gaussian distribution can

be used to represent the ΔI_o values with a mean value of $\Delta I_o = 0$ and $SDM_o = \sqrt{2}\ SDM_{t<0}$ (i.e., if our study was done over again many times, many ΔI_o values would be obtained with the average equal to $\Delta I_o = 0$ and a spread represented by SDM_o). A comparison will be made between the distribution of ΔI_o's for the uncorrelated situation and the ΔI's calculated in this survey.

If a significant number of AKR onsets is triggered by Type-III bursts as to imply a relationship, one would expect ΔI above probable uncorrelated intensity increases, ΔI_o. Thus, a Type-III/AKR correlation exists if ΔI is 2 SDM_o above $\Delta I_o = 0$ (where the range of highly probable ΔI_o values falls within 2 SDM_o of $\Delta I_o = 0$). However, if no Type-III triggered AKR are detected in $t > 0$, a Type-III/AKR relationship does not exist and $\Delta I \cong \Delta I_o$. Thus, no correlation exists between Type-III bursts and AKR if ΔI is within 2 SDM_o of $\Delta I_o = 0$ (or in other words, no correlation exists if ΔI is within the range of highly probable ΔI_o values).

In effect, when ΔI is 2 SDM_o above $\Delta I_o = 0$, the ΔI value can no longer be considered compatible with the values obtained from the uncorrelated case. Such large intensity increases imply that AKR is being triggered by Type-III bursts and that a Type-III/AKR correlation exists.

Again, the epoch analysis is done for three different frequencies. For each event, the 100-kHz, 188-kHz and 513-kHz spectral density data from ISEE-3 is subtracted from the 100-kHz, 178-kHz and 500-kHz spectral density data from IMP-8, respectively. It is assumed that the Type-III intensity form doesn't change substantially from 178 kHz to 188 kHz and from 500 kHz to 513 kHz.

IV. RESULTS

The superposed epoch analysis was performed at the three frequencies mentioned. Figure 11 shows the results of the analysis. In the figure, the log of the spectral density is plotted vs. time, with $t = 0$ being the start of the Type-III burst's passage. At 100 kHz large intensity increases are not seen in the second hour ($t > 0$). The first hour average intensity (average of background) is 6.04×10^{-15} $V^2 m^{-2} Hz^{-1}$ while the second hour average intensity (average of background and any AKR occurrences) is 5.12×10^{-15} $V^2 m^{-2} Hz^{-1}$. At 178 kHz, an increase in intensity is found with the first hour average intensity at 4.07×10^{-14} $V^2 m^{-2} Hz^{-1}$ and the second hour average intensity at 6.10×10^{-14} $V^2 m^{-2} Hz^{-1}$. An intensity increase is also seen at 500 kHz with the first hour average intensity at 4.7×10^{-18} $V^2 m^{-2} Hz^{-1}$ and the second hour average intensity at 18.3×10^{-18} $V^2 m^{-2} Hz^{-1}$.

Note, at 500 kHz, the background period picked is slightly less than an hour while the remaining period after $t = 0$ is slightly over an hour. This small period shift is because the 2-hour period at 100 kHz has the start of the Type-III burst, $t = 0$, at center. Type-III radiation arrives earlier at higher frequencies, thus $t = 0$ is shifted to an earlier position in the 2 hour period at 500 kHz.

The standard deviation of the mean for the first hour ($SDM_{t<0}$) is calculated from the epoch analysis results. This value is defined as $s/\sqrt{n}$ where s is the sample standard deviation of the first hour and n is the number of data points in each first hour region. Table 1 shows the average intensity in each hour ($\overline{I}_{t<0}$ and $\overline{I}_{t>0}$) along with the first hour's standard deviation ($S_{t<0}$) and standard deviation of the mean ($SDM_{t<0}$). From these $SDM_{t<0}$ values, SDM_o can be calculated. The SDM_o values are 1.06×10^{-15} $V^2m^{-2}Hz^{-1}$, 0.48×10^{-14} $V^2m^{-2}Hz^{-1}$ and 2.94×10^{-18} $V^2m^{-2}Hz^{-1}$ for 100 kHz, 178 kHz and 500 kHz, respectively. As mentioned, if no Type-III/AKR correlation exists, one would expect our intensity increases to fall within 2 SDM_o of $\Delta I_o = 0$ where $\Delta I_o = 0$ is the average intensity increase when no correlation exists. However, if ΔI is above 2 SDM_o of $\Delta I_o = 0$, the gain in intensity seen after t = 0 (the passage time of the Type-III burst) indicates increased onsets of AKR and implies a Type-III/AKR correlation exists.

At 178 kHz, the best estimate of ΔI, where $\Delta I = \overline{I}_{t>0} - \overline{I}_{t<0}$, is $\Delta I = 2.03 \times 10^{-14}$ $V^2m^{-2}Hz^{-1}$. This value is 4.23 SDM_o greater than $\Delta I_o = 0$ and indicates that large intensity increases are found after t = 0. This implies that a Type-III/AKR correlation exists.

At 500 kHz, the best estimate of ΔI is $\Delta I = 13.60 \times 10^{-18}$ $V^2m^{-2}Hz^{-1}$. This value is 4.63 SDM_o greater than $\Delta I_o = 0$ and, again, implies that a Type-III/AKR correlation exists.

The intensity increases at 178 kHz and 500 kHz agree with Calvert's results that Type-III bursts trigger AKR and that the

simultaneous occurrence of the two emissions is not just a chance accident, but is the result of a "cause-and-effect" relationship.

A question that must be asked is whether the intensity increases at 178 kHz and 500 kHz could have come from background fluctuations alone. In other words, what is the probability that these intensity increases are not the result of Type-III stimulated AKR but result from some random emission that, by chance, happens to occur more often in the second hour? The probability of random emissions causing the intensity jumps is low. Using the central limit theorem of statistics and the best estimate for ΔI, the probability is calculated to be less than 10^{-4} at 178 kHz and less than 10^{-5} at 500 kHz. Since this probability is small, a reasonable conclusion is that AKR is being consistently triggered by Type-III bursts in the second hour causing the intensity level to rise.

At 100 kHz, the best estimate of ΔI falls within 2 SDM_o of $\Delta I_o = 0$. No large intensity increases are seen for $t > 0$ implying, at this frequency, that few (if any) Type-III related AKR onsets occurred in the 200-event sample. This result implies the Type-III/AKR correlation is not strong at this frequency.

The gain of each frequency can be calculated by noting the intensity changes in the second hour as compared to the first. At 100 kHz, the intensity actually decreases slightly in the $t > 0$ region, thus a -0.7 dB gain is found. The gain at 178 kHz is 1.9 dB while at 500 kHz, the gain is 5.9 dB. According to theory, if all incoming Type-III bursts stimulated an AKR onset, the epoch analysis

would yield a gain above background of about 80 dB. Since the gains actually observed are fractions of this, an AKR triggering probability for a Type-III burst can be calculated at each frequency (i.e., if half the Type-III bursts trigger AKR, a 40 dB gain would be calculated in the epoch analysis, yielding a triggering probability of 40 dB/80 dB or 0.5). Table 2 shows these probabilities at each frequency. The largest probability is found at 500 kHz with a triggering probability equal to .074, implying 7.4% of incoming Type-III bursts stimulate AKR.

The power spectrum is shown in Figure 12 for the pre-event and post-event power fluxes. Note that the post-event's spectrum is more intense than the pre-event's, indicating an intensity increase after the passage of the burst. Also, the power output at 500 kHz shows that the post-event level is almost a factor of 3 times larger than the pre-event level, while at 178 kHz, the post-event level is a factor of 1.5-2 times larger than the pre-event levels. The frequency integrated power flux increase is, then, 1.19×10^{-11} Wm^{-2}, which is a 50% change in frequency integrated power flux output from pre-event levels.

V. CONCLUSION

The superposed epoch analysis performed on Type-III radio bursts indicate substantial intensity increases after the arrival of the Type-III bursts. These intensity increases imply an increase in the occurrence of AKR after the arrival of a Type-III burst.

Intensity increases after $t = 0$ were found at both 178 kHz and 500 kHz. These increases are well above the increases expected if no Type-III/AKR correlation existed. These large intensity increases in the $t > 0$ region indicate that Type-III correlated onsets of AKR occurred and a Type-III/AKR correlation exists.

The power spectrum also shows an increase in intensity from pre-event to post-event power fluxes. This power flux increase adds to the mounting evidence of a Type-III/AKR correlation.

By noting the intensity gain from the first to second hour, an AKR triggering probability for an incoming Type-III burst can be determined at each of the frequencies studied. At 500 kHz, a .074 probability exists indicating about 7.4% of incoming Type-III bursts stimulate AKR.

All of these conclusions back Calvert's hypothesis that incoming Type-III bursts stimulate AKR. This survey indicates close to 10% of incoming Type-III bursts stimulate AKR (as indicated by the 500-kHz triggering probability) and shows an external (outside earth) source besides cosmic background can cause AKR stimulation.

Table 1. Superposed Epoch Analysis Results

	$\bar{I}_{t<0}$ $(\frac{V}{m})^2 \frac{1}{Hz}$	$s_{t<0}$ $(\frac{V}{m})^2 \frac{1}{Hz}$	$SDM_{t<0}$ $(\frac{V}{m})^2 \frac{1}{Hz}$	$\bar{I}_{t>0}$ $(\frac{V}{m})^2 \frac{1}{Hz}$
100 kHz	6.04×10^{-15}	2.50×10^{-15}	$.75\times10^{-15}$	5.13×10^{-15}
178 kHz	4.07×10^{-14}	1.07×10^{-14}	$.34\times10^{-14}$	6.10×10^{-14}
500 kHz	4.74×10^{-18}	5.51×10^{-18}	2.08×10^{-18}	18.34×10^{-18}

The $t < 0$ average intensity, standard deviation and standard deviation of the mean along with the $t > 0$ average intensity is listed for each frequency.

Table 2. AKR Triggering Probability for Type-III Bursts

Frequency	Probability
100 kHz	-0.009
178 kHz	0.024
500 kHz	0.074

The AKR triggering probability for an incoming Type-III burst at each frequency is listed.

Figure 1 A qualitative view of the AKR ray paths. The source is along the auroral field line with ray refractions occurring from the propagation cutoff surface and plasmasphere.

A-G74-51

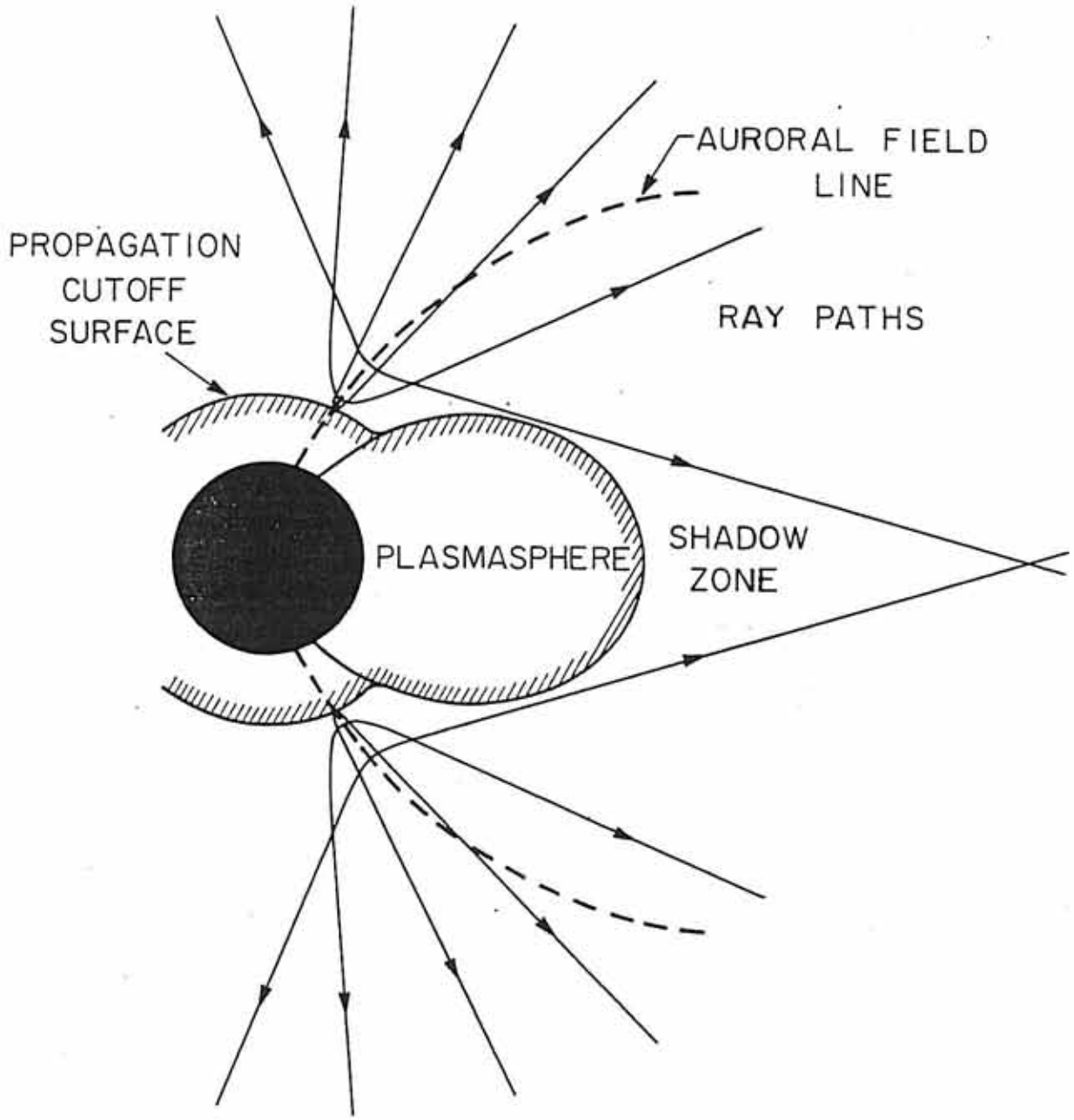

Figure 1

Figure 2 AKR emissions detected from the IMP-6 satellite. Note the bursty nature of the emission.

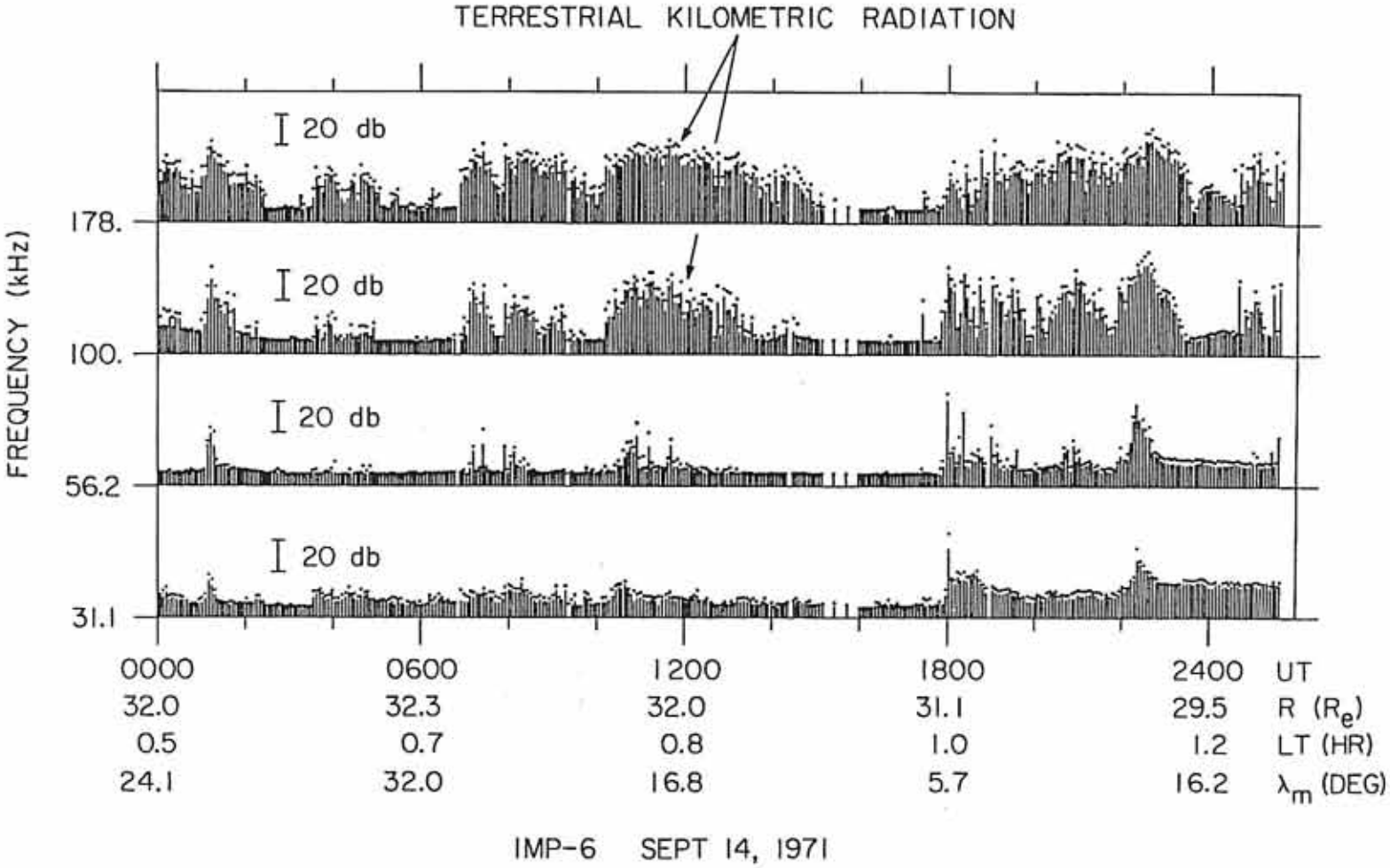
TERRESTRIAL KILOMETRIC RADIATION
I 20 db
I 20 db
I 20 db
I 20 db
FREQUENCY (kHz)
178.
100.
56.2
31.1
0000 0600 1200 1800 2400 UT
32.0 32.3 32.0 31.1 29.5 R (Re)
0.5 0.7 0.8 1.0 1.2 LT (HR)
24.1 32.0 16.8 5.7 16.2 λm (DEG)
IMP-6 SEPT 14, 1971

Figure 2

Figure 3 The detailed fine structure of AKR as detected by ISEE-1 is shown. Note the narrow band emissions in the bottom spectrogram.

B-G79-407

UNIVERSITY OF IOWA PLASMA WAVE EXPERIMENT

DECEMBER 28, 1977 DAY 362 ORBIT 28

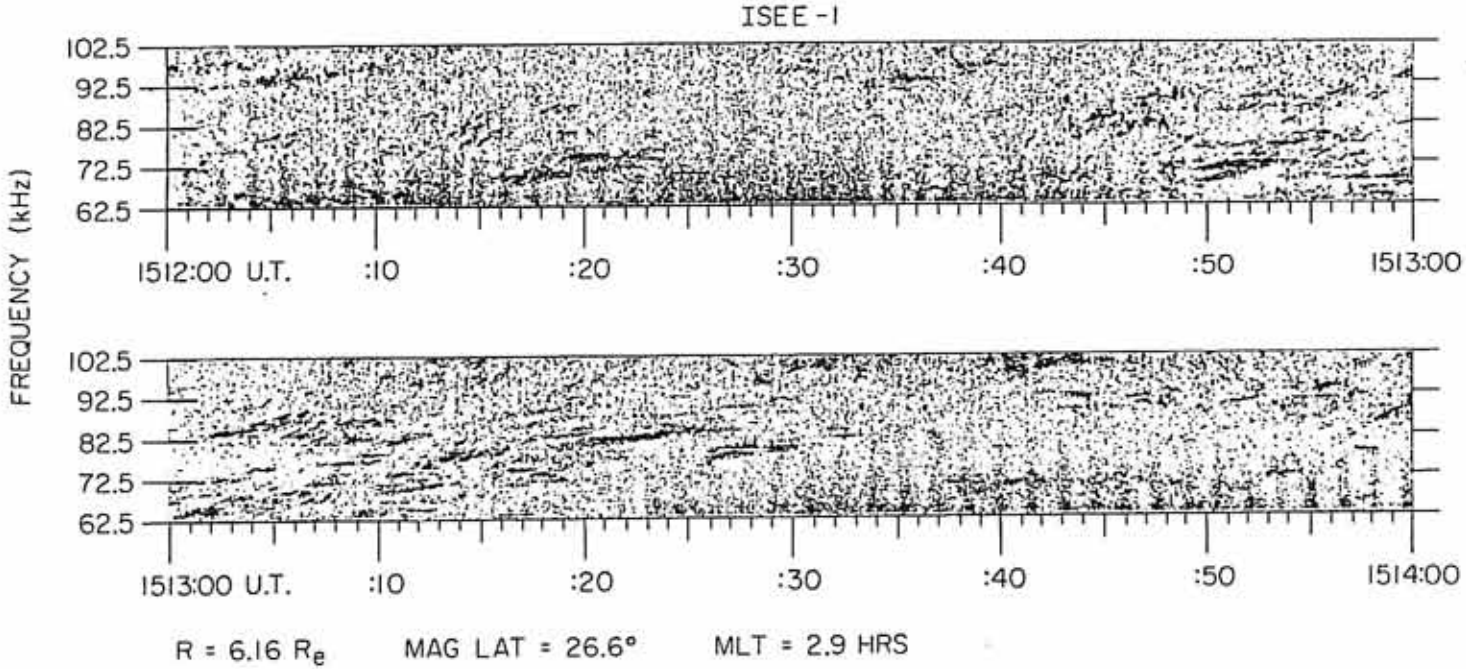

R = 6.16 R_e MAG LAT = 26.6° MLT = 2.9 HRS

Figure 4 A qualitative radial profile of electromagnetic radiation (Type-III bursts) and plasma oscillations generated from solar flare electrons.

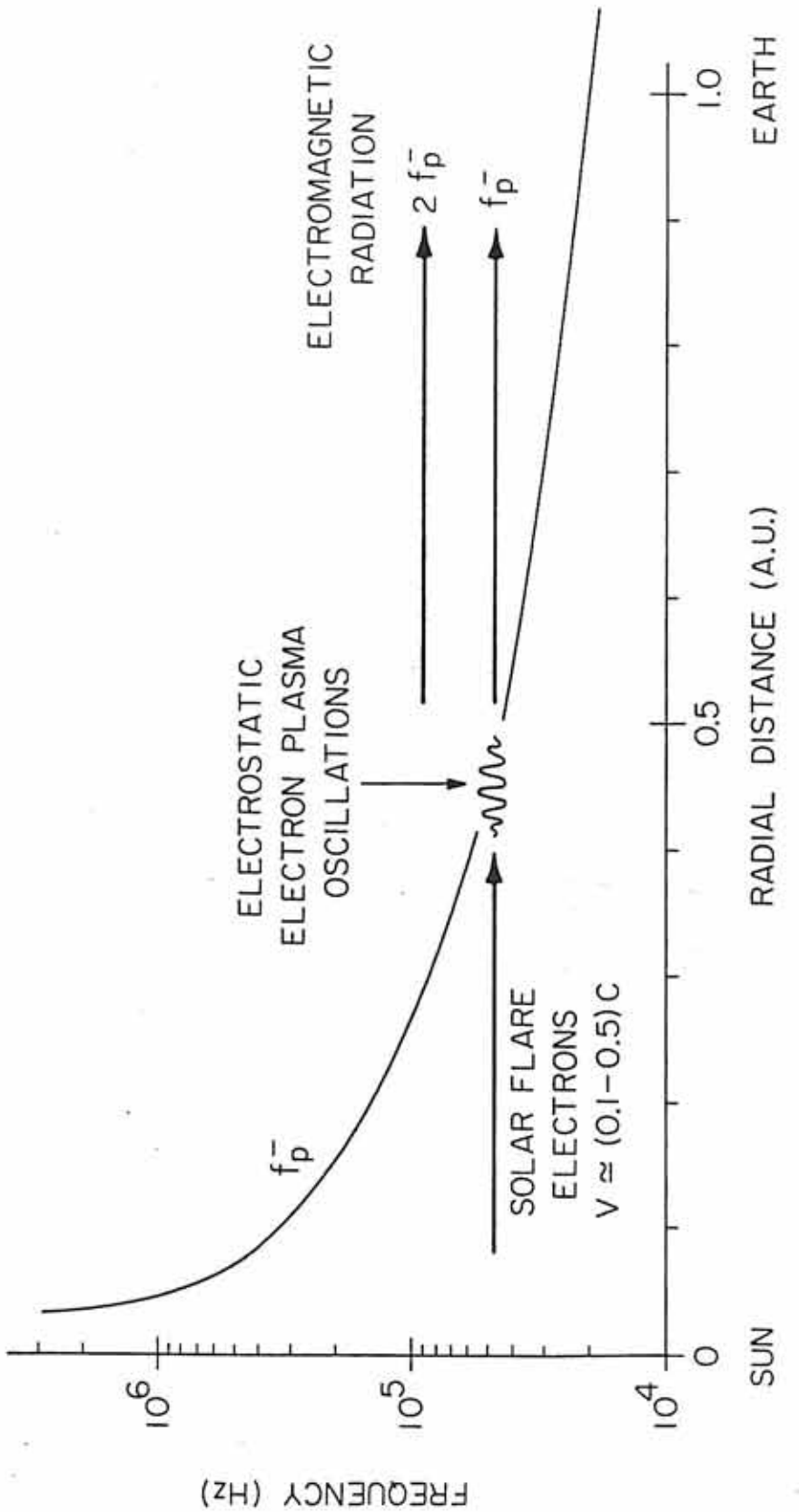
B-G79-801
ELECTROMAGNETIC RADIATION
2 f_p^-
f_p^-
ELECTROSTATIC ELECTRON PLASMA OSCILLATIONS
f_p^-
SOLAR FLARE ELECTRONS
V ≃ (0.1-0.5)C
FREQUENCY (Hz)
10^6
10^5
10^4
SUN
0
0.5
1.0
EARTH
RADIAL DISTANCE (A.U.)

Figure 4

Figure 5 A Type-III radio burst as detected by Helios-2. The radio emission is seen at 178 kHz and 100 kHz. Electron plasma oscillations generated by solar flare electrons in the solar wind are seen at 56.2 kHz and 31.1 kHz.

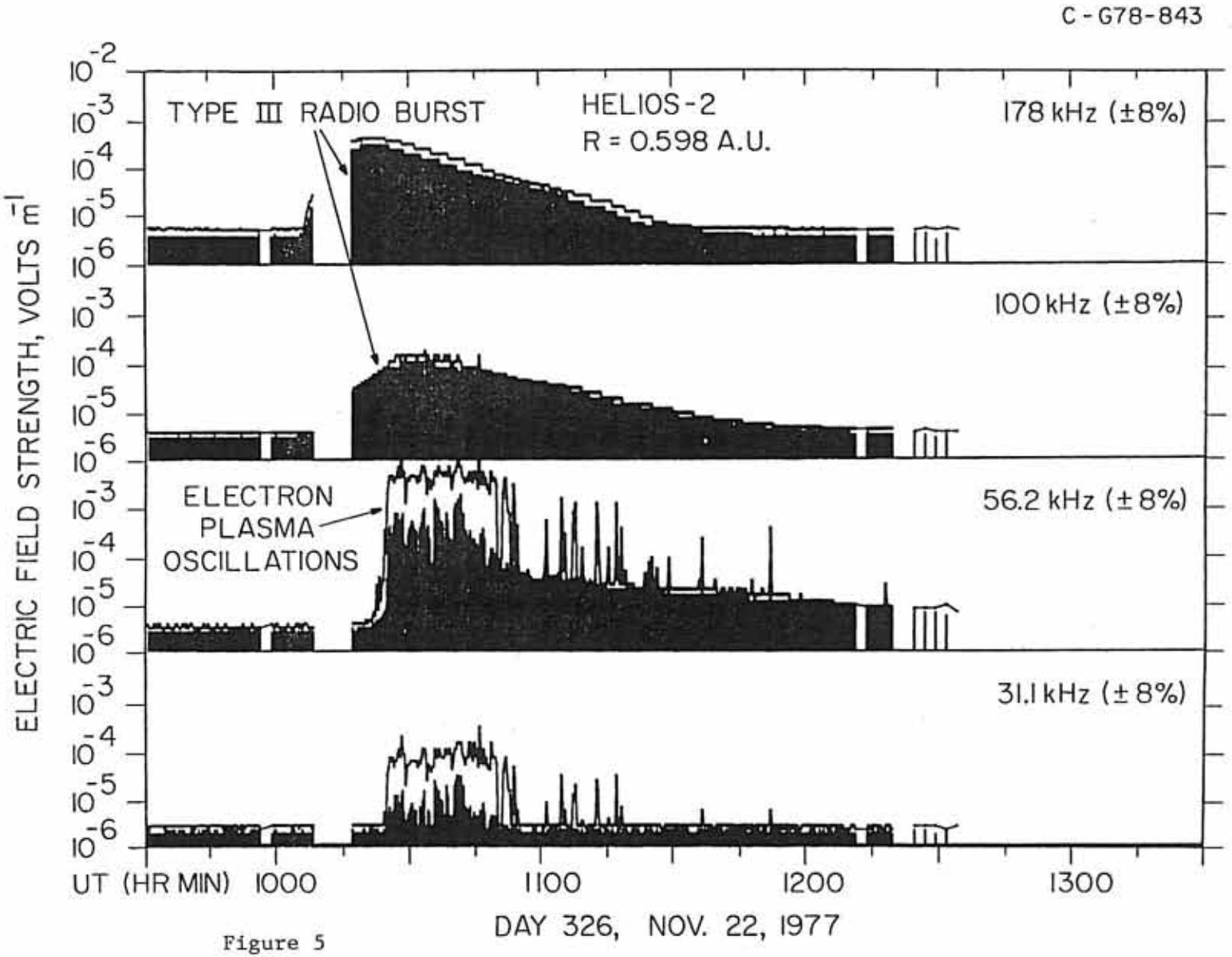
C-G78-843
TYPE III RADIO BURST
HELIOS-2
R = 0.598 A.U.
178 kHz (±8%)
100 kHz (±8%)
ELECTRON
PLASMA
OSCILLATIONS
56.2 kHz (±8%)
31.1 kHz (±8%)
ELECTRIC FIELD STRENGTH, VOLTS m⁻¹
UT (HR MIN) 1000
1100
1200
1300
DAY 326, NOV. 22, 1977

Figure 5

Figure 6 An ISEE-1 spectrogram showing a Type-III burst occurring on November 17, 1979. Note the high to low frequency drift.

A-G84-1362

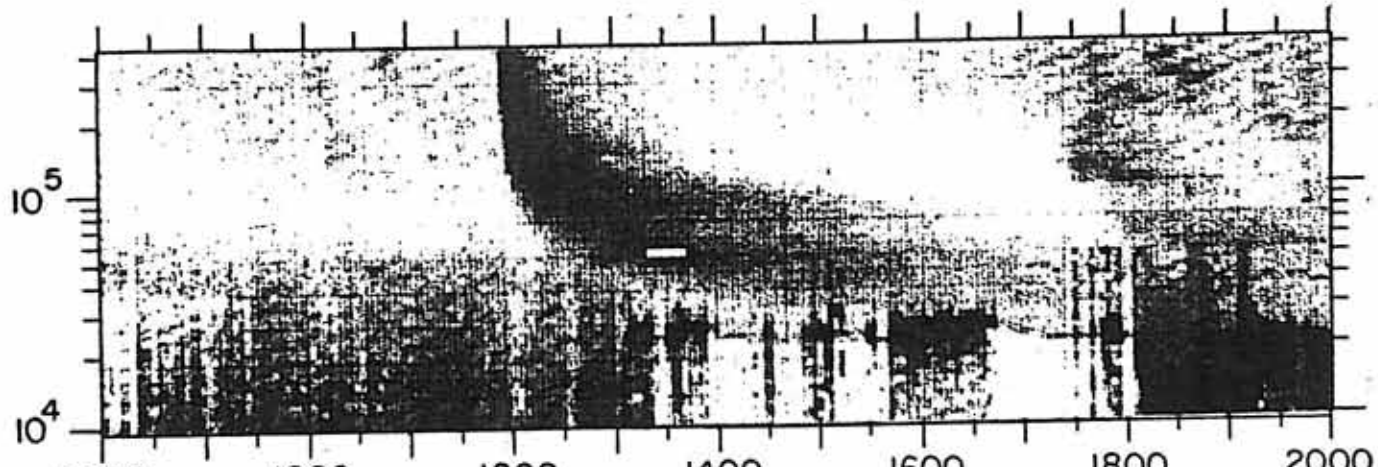

UT	0800	1000	1200	1400	1600	1800	2000
R (RE)	20.594	18.197	18.901	19.605	20.308	20.985	21.519
MLAT	13.84	35.26	28.99	22.73	16.46	9.95	2.68
MLT	8.92	8.99	8.97	8.95	8.93	8.92	8.95
ORBIT	0	317	317	317	317	317	317
L	0.0	0.0	0.0	0.0	0.0	0.0	0.0

Figure 7 An ISEE-1 spectrogram showing Type-III bursts and simultaneous AKR occurrences at 1630 and 2200 UT.

A-G81-244-1

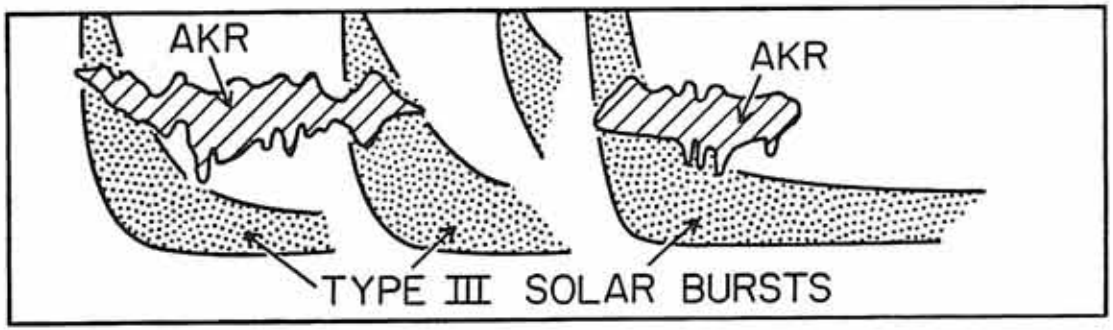

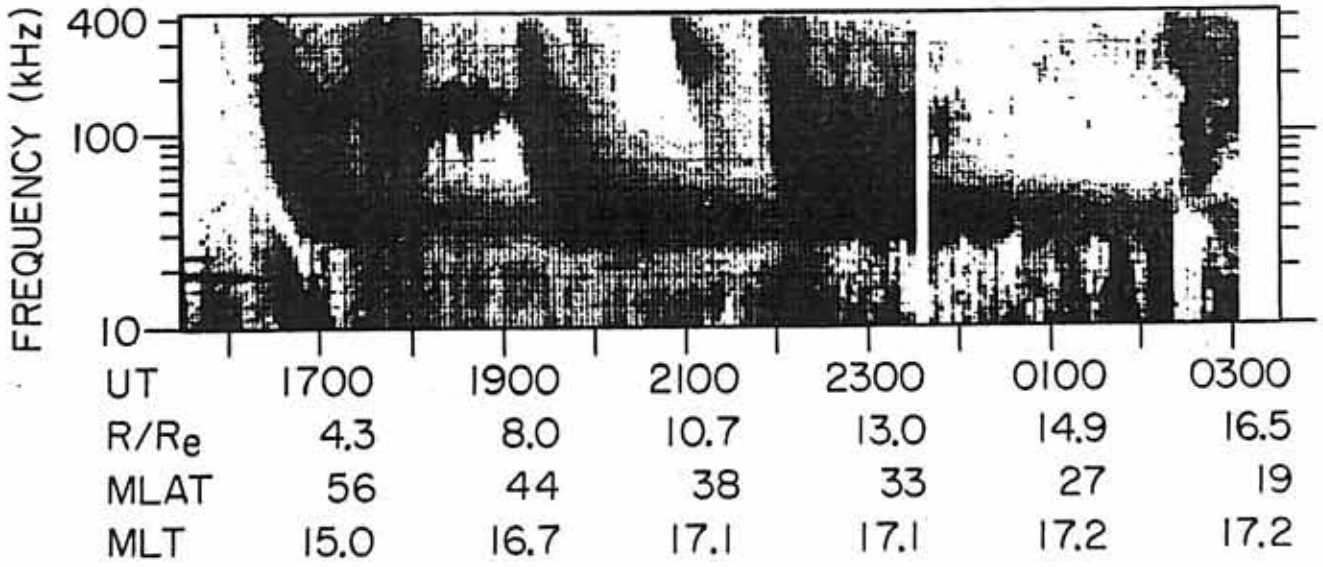

ISEE-1 3-4 JULY 1979

Figure 8 The IMP-8 spectral density is compared to the ISEE-3 spectral density for the isolated Type-III burst occurring on Sept. 6, 1978, at 5:59 UT at 100 kHz.

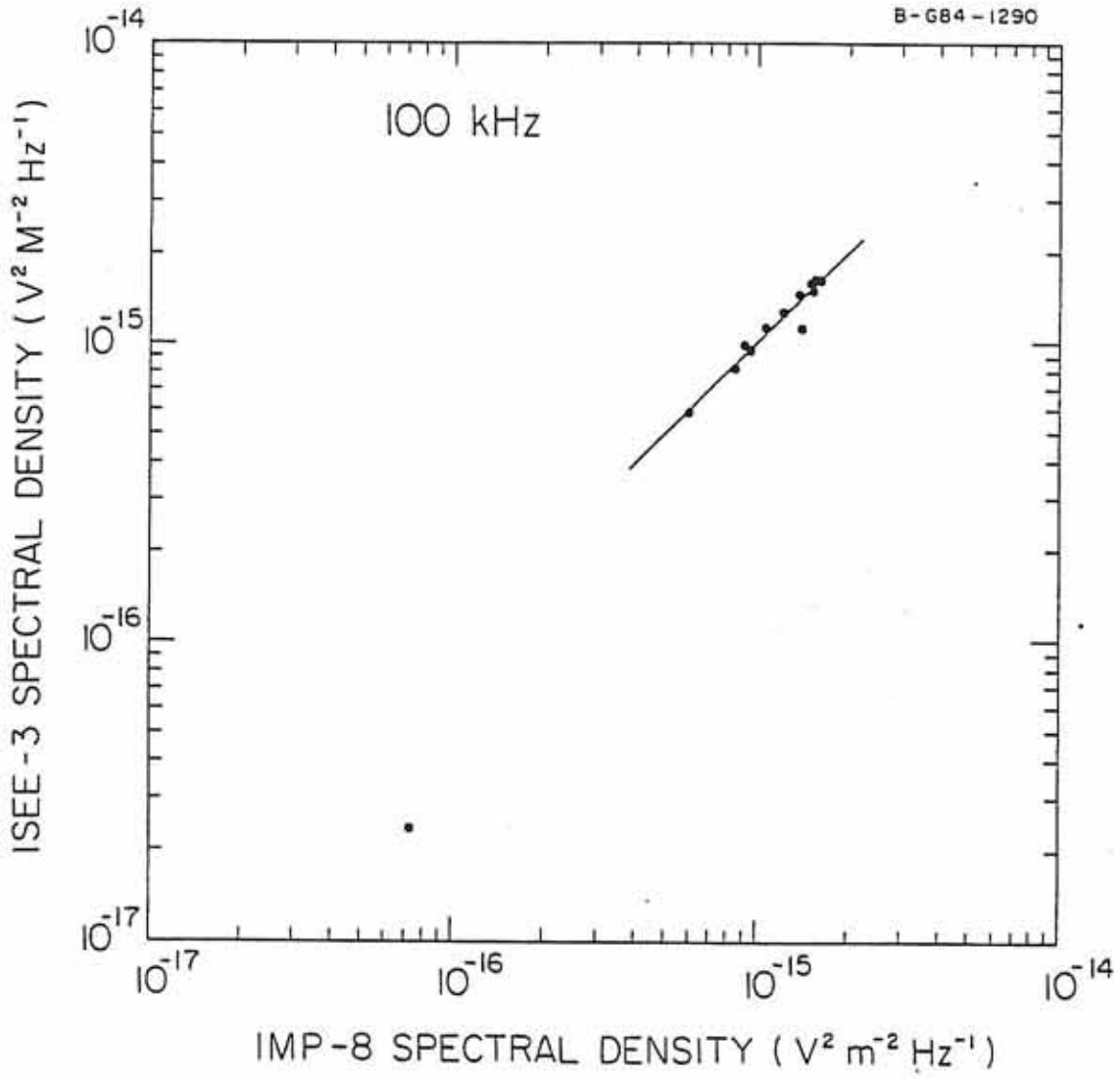
B-G84-1290
100 kHz
ISEE-3 SPECTRAL DENSITY (V² M⁻² Hz⁻¹)
IMP-8 SPECTRAL DENSITY (V² m⁻² Hz⁻¹)
10⁻¹⁴
10⁻¹⁵
10⁻¹⁶
10⁻¹⁷
10⁻¹⁷
10⁻¹⁶
10⁻¹⁵
10⁻¹⁴

Figure 8

Figure 9 The IMP-8 spectral density is compared to the ISEE-3 spectral density for the isolated Type-III burst occurring on June 26, 1979, at 14:55 UT at 178 kHz.

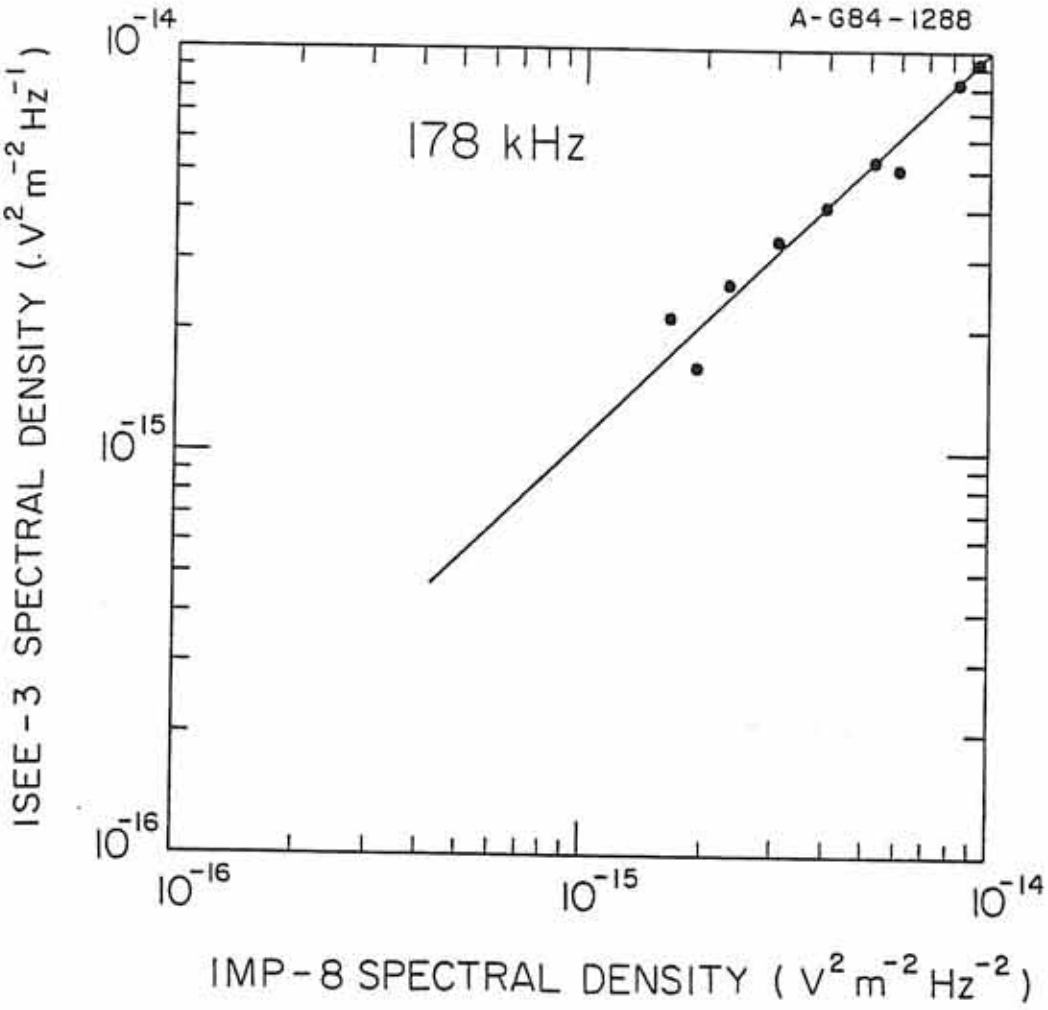
A-G84-1288
178 kHz
ISEE-3 SPECTRAL DENSITY ($V^2 m^{-2} Hz^{-1}$)
IMP-8 SPECTRAL DENSITY ($V^2 m^{-2} Hz^{-2}$)
10^{-14}
10^{-15}
10^{-16}
10^{-16}
10^{-15}
10^{-14}

Figure 9

Figure 10 The IMP-8 spectral density is compared to the ISEE-3 spectral density for the isolated Type-III burst occurring on June 26, 1979, at 14:55 UT at 500 kHz.

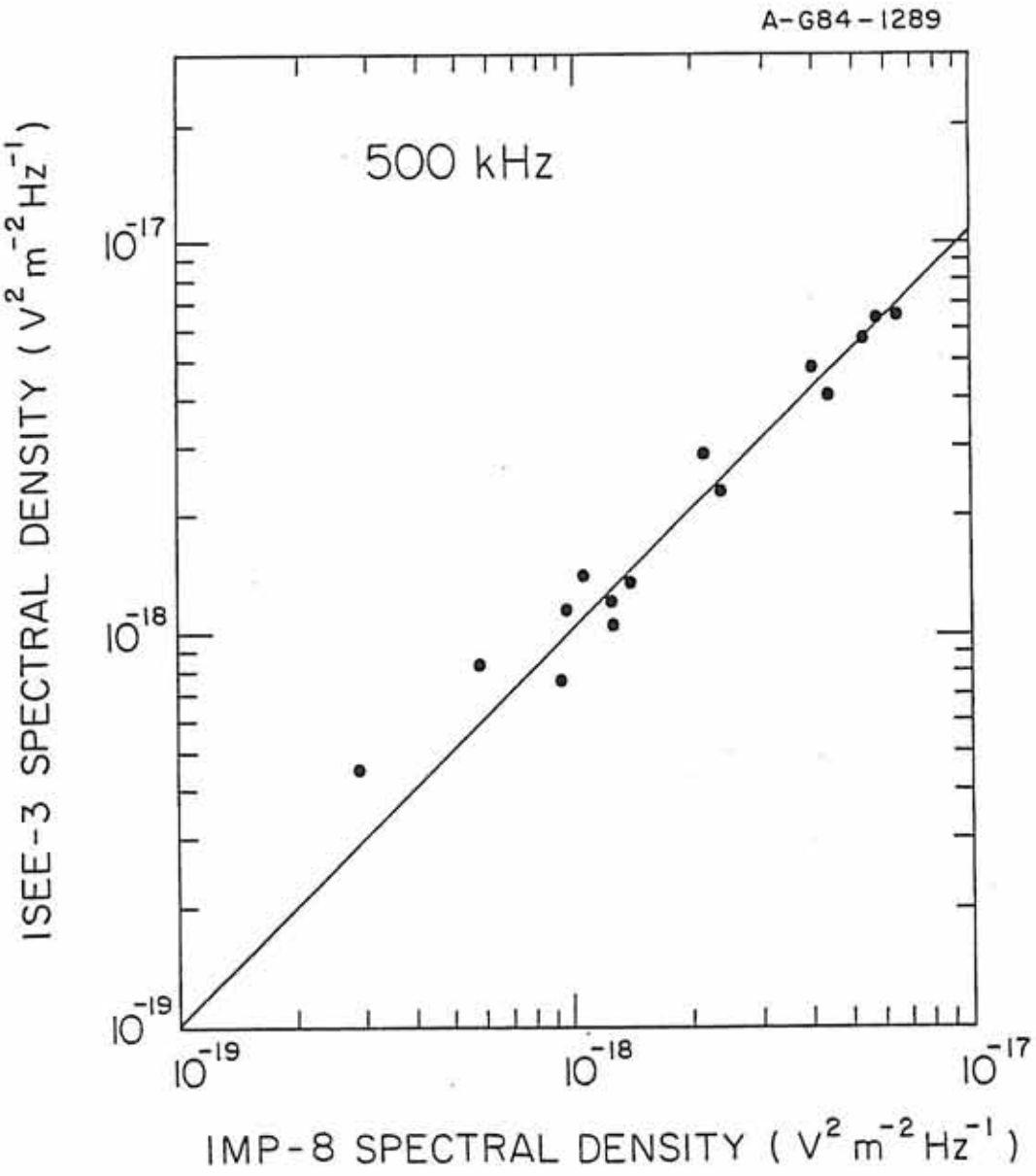
A-G84-1289
500 kHz
ISEE-3 SPECTRAL DENSITY (V² m⁻² Hz⁻¹)
IMP-8 SPECTRAL DENSITY (V² m⁻² Hz⁻¹)
10⁻¹⁷
10⁻¹⁸
10⁻¹⁹
10⁻¹⁹
10⁻¹⁸
10⁻¹⁷

Figure 10

Figure 11 The results of the superposed epoch analysis at 100-kHz, 178-kHz and 500-kHz frequencies are shown. The t = 0 point represents the start of the Type-III burst's passage for all events.

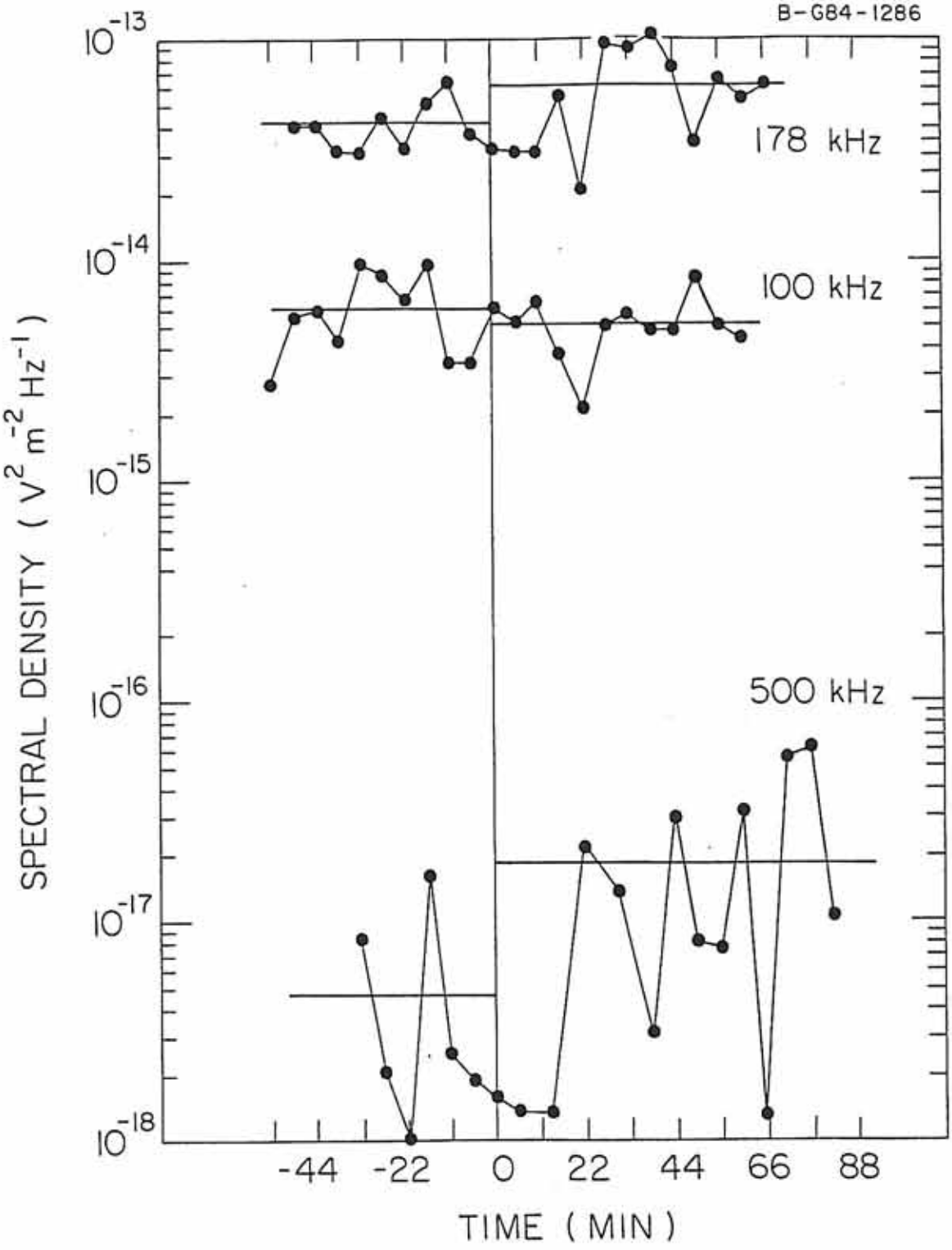
B-G84-1286
178 kHz
100 kHz
500 kHz
SPECTRAL DENSITY (V² m⁻² Hz⁻¹)
10⁻¹³
10⁻¹⁴
10⁻¹⁵
10⁻¹⁶
10⁻¹⁷
10⁻¹⁸
-44
-22
0
22
44
66
88
TIME (MIN)

Figure 12 The power spectrum is shown for the pre-Type-III event and post-Type-III event power fluxes.

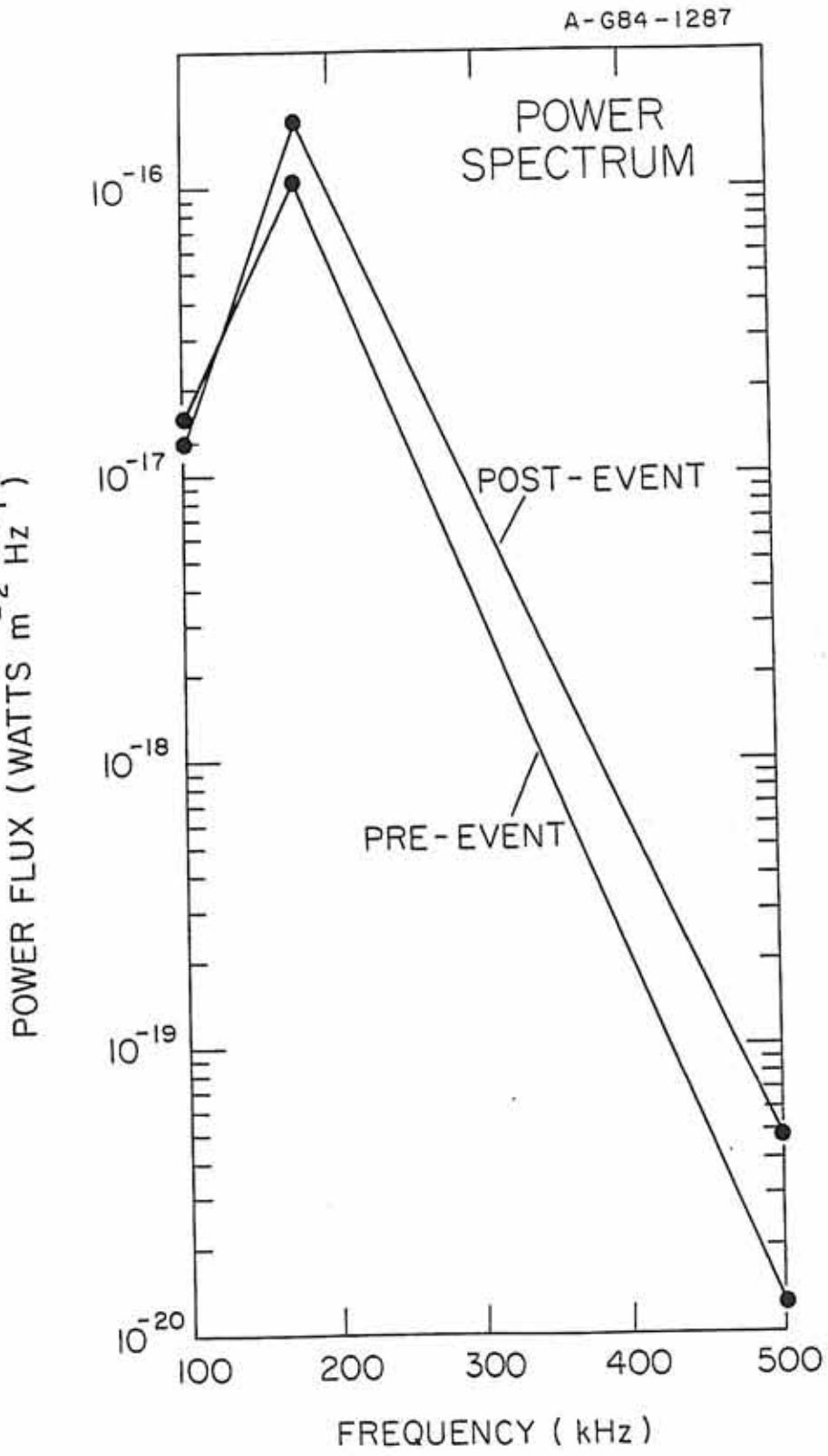
A-G84-1287
POWER SPECTRUM
POST-EVENT
PRE-EVENT
POWER FLUX (WATTS m^{-2} Hz^{-1})
10^{-16}
10^{-17}
10^{-18}
10^{-19}
10^{-20}
100
200
300
400
500
FREQUENCY (kHz)

Figure 12

REFERENCES

Benson, R. F., and W. Calvert, ISIS-1 observations at the source of auroral kilometric radiation, Geophys. Res. Lett., 6, 479-482, 1979.

Benson, R. F., W. Calvert, and D. M. Klumpar, Simultaneous wave and particle observations in the auroral kilometric radiation source region, Geophys. Res. Lett., 7, 959-962, 1980.

Calvert, W., The stimulation of auroral kilometric radiation by Type-III solar radio bursts, Geophys. Res. Lett., 8, 1091, 1981a.

Calvert, W., The signature of auroral kilometric radiation on ISIS-1 ionograms, J. Geophys. Res., 86, 76-82, 1981b.

Calvert, W., The auroral plasma cavity, Geophys. Res. Lett., 8, 919, 1981c.

Calvert, W., A feedback model for the source of auroral kilometric radiation, J. Geophys. Res., 87, 8199, 1982.

Dunckel, N., B. Ficklin, L. Rorden, and R. A. Helliwell, Low-frequency noise observed in the distant magnetosphere with OGO-1, J. Geophys. Res., 75, 1854-1862, 1970.

Fainberg, J., and R. G. Stone, Satellite observations of Type-III solar radio bursts at low freuqneices, Space Sci. Rev., 16, 145-188, 1974.

Gallagher, D. L., and D. A. Gurnett, Auroral kilometric radiation: Time-averaged source location, J. Geophys. Res., 84, 6501-6509, 1979.

Gurnett, D. A., The earth as a radio source: Terrestrial kilometric radiation, J. Geophys. Res., 79, 4227-4238, 1974.

Gurnett, D. A., and J. L. Green, On the polarization and origin of auroral kilometric radiation, J. Geophys. Res., 83, 689-696, 1978.

Knoll, R., G. Epstein, S. Hoang, G. Huntzinger, J. L. Steinberg, J. Fainberg, F. Grena, S. R. Mosier, and R. G. Stone, The 3-dimensional radio mapping experiment (SBH) on ISEE-C, IEEE Trans. Geosci. Electron., GE-16, 199-204, 1978.

Lin, R. P., D. W. Potter, D. A. Gurnett, and F. L. Scarf, Energetic electrons and plasma waves associated with a solar Type-III radio burst, Astrophys. J., 251, 364-373, 1981.

Melrose, D. B., An interpretation of Jupiter's decametric radiation and the terrestrial kilometric radiation as direct amplified gyroemission, Astrophys. J., 207, 651, 1976.

Omidi, N., and D. A. Gurnett, Growth rate calculations of auroral kilometric radiation using the relativistic resonance condition, J. Geophys. Res., 87, 2377-2383, 1982.

Scarf, F. L., R. W. Fredricks, D. A. Gurnett, and E. J. Smith, The ISEE-C plasma wave investigation, IEEE Trans. Geosci. Electron., GE-16, 191-195, 1978.

Wild, J. P., Observations of the spectrum of high-intensity solar radiation at metre wavelengths, Aust. J. Sci., 3, 541-577, 1950.

Wu, C. S., and L. C. Lee, A theory of the terrestrial kilometric radiation, Astrophys. J., 230, 621-626, 1979.